

INTEGRAL OBSERVATIONS OF CYGNUS X-3

Linnea Hjalmarsdotter¹, A. A. Zdziarski², A. Paizis^{3,4}, V. Beckmann^{4,5}, and O. Vilhu^{1,3}¹ Observatory, P.O. Box 14, 00014 University of Helsinki, Finland² Centrum Astronomiczne im. M. Kopernika, Bartycka 18, 00-716 Warsaw, Poland³ INTEGRAL Science Data Center, Chemin d'Écogia 16, CH-1290 Versoix, Switzerland⁴ CNR-IASF, Sezione di Milano, Via Bassini 15, 20133 Milano, Italy⁴ NASA Goddard Space Flight Center, Code 661, Greenbelt, MD 20771, USA⁵ Joint Center for Astrophysics, Department of Physics, University of Maryland, Baltimore County, MD 21250, USA

ABSTRACT

The peculiar X-ray binary Cygnus X-3 has been observed on several occasions with the X/ γ -ray instruments on board *INTEGRAL*. We have collected data from available public and Galactic Plane Scan observations between December 2002 and December 2003 and summed them together into two broad-band spectra, representing different physical spectral states of the source. We have fitted the two spectra with models including Comptonization and Compton reflection, similar to those found for black-hole binaries at high accretion rates.

Key words: gamma rays: observations – radiation mechanisms: non-thermal – stars: individual: Cyg X-3 – X-rays: binaries – X-rays: general – X-rays: stars.

1. INTRODUCTION

Cyg X-3 is an enigmatic X-ray binary that ever since its discovery 38 years ago, in 1966 (Giacconi et al. 1967), has evaded simple classification. Its 4.8 hr orbital period is typical of a low-mass system, but infrared observations have shown the donor to be a high-mass Wolf-Rayet star (e.g., van Kerkwijk et al. 1992; 1996). The nature of the compact object is uncertain; it may be either a neutron star or a black hole (e.g., Schmutz et al. 1996; Ergma & Yungelson 1998; Stark & Saia 2003). The system, located at a distance of ~ 9 kpc (e.g., Predehl et al. 2000), is embedded in such a dense wind from the donor star that most of its intrinsic emission is strongly obscured. Still, its hard X-rays and γ -rays can be observed unimpeded, making it a very good target for *INTEGRAL*.

As an X-ray source, Cyg X-3 is one of the brightest in the Galaxy. It displays states with high and low level of emission at $\lesssim 10$ keV (e.g. White & Holt 1982; Watanabe et al. 1994). The observed EF_E spectrum in the high/soft state peaks at a few keV and is highly variable, whereas in the low/hard state the peak is at ~ 20 keV and there is

less variability. At the other end of the spectrum, Cyg X-3 is the strongest radio source among the X-ray binaries and shows huge radio outbursts associated with relativistic jets. The radio activity and the production of the jets are closely linked with the X-ray emission and the different X-ray states (McCollough et al. 1999; Choudhury et al. 2002).

It is believed that Cyg X-3 shows so many unique properties because it is in a very short-lived transitional phase of binary evolution. It is therefore possible that the system represents a stage of evolution that will be the fate of many of the massive X-ray binaries observed today. If this is the case, an understanding of this peculiar source could prove to have broad implications for high-mass X-ray binaries in general.

2. OBSERVATIONS AND DATA ANALYSIS

Cyg X-3 has been observed on several occasions with all three X/ γ -ray instruments aboard *INTEGRAL*. The most extensive observations were carried out during the *INTEGRAL* performance verification phase observations of the Cygnus region in December 2002. (The data for Rev. 23 are described in Vilhu et al. 2003, hereafter V03.) Cyg X-3 has also been in the FOV in several of the Galactic Plane Scans (GPS) carried out during 2003. Due to the large variability of the source (see Fig. 1), a simple co-adding of all available observations will not represent a physical spectrum of Cyg X-3. It is true, however, that the spectral state of this source can be roughly determined by the flux level in 1.5–12 keV X-rays as measured by the All Sky Monitor (ASM) on board *RXTE*. Here, we have therefore grouped the observations based on the *RXTE*/ASM count rate and combined the selected science windows to build two co-added spectra of Cyg X-3, representing different spectral states. The dates for the observations are listed in Table 1 and also indicated in Fig. 1 together with the corresponding flux levels as seen by *RXTE*/ASM.

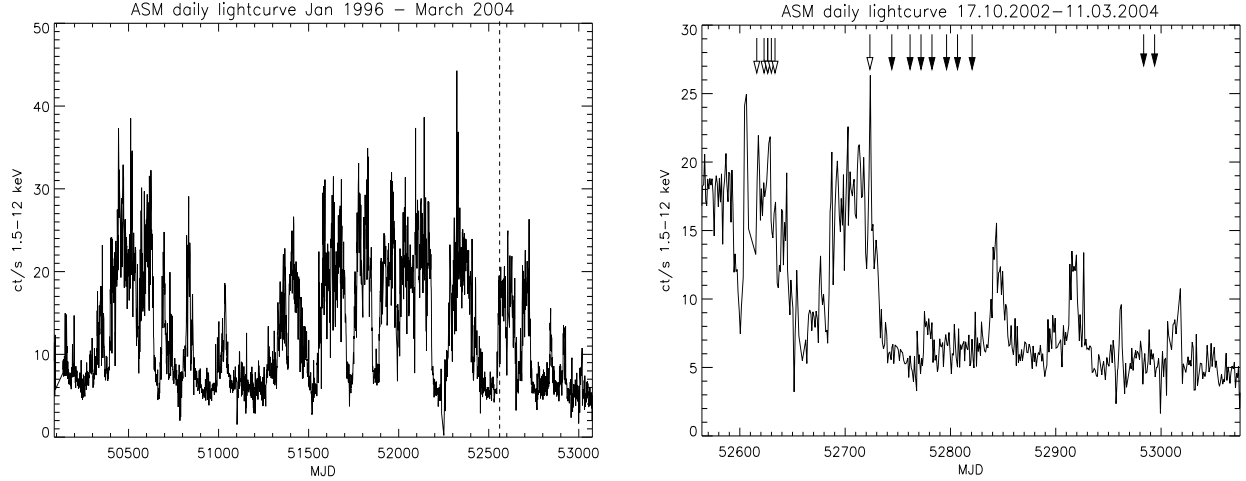


Figure 1. Left panel: The RXTE/ASM lightcurve since launch of RXTE in January 1996 until March 2004. The launch of INTEGRAL is shown by a vertical line. Right panel: An enlarged portion of the same lightcurve representing the lifetime of INTEGRAL. The times of the INTEGRAL observations are shown as arrows. Observations indicated with open arrows were used to construct the ‘high’ state spectrum and observations indicated by filled arrows to construct the ‘low’ state spectrum. It is clear from a comparison with the long-term RXTE/ASM lightcurve that the source has not been in a very high state since the launch of INTEGRAL.

Table 1. Data from the listed revolutions were used to create the ‘high’ state spectrum. The dates represent the start date of each revolution. The same dates are indicated by open arrows in Fig. 1. Effective exposure times in ksec are given for each instrument per revolution and in total.

Rev.	start date	JEM-X	ISGRI	SPI
19	2002 – 12 – 09	36	36	–
20	2002 – 12 – 12	17	17	133
21	2002 – 12 – 15	–	–	180
22	2002 – 12 – 18	–	–	161
23	2002 – 12 – 21	82	82	169
54	2003 – 03 – 24	2	2	9
Total	exposure time	137	137	652

2.1. JEM-X

The observations were performed with the second (JEM-X2) of the two identical X-ray monitors. The JEM-X and ISGRI data were analysed using ISDC’s (Courvoisier et al. 2003) Offline Standard Analysis (OSA) software version 3.0. The data were taken from 54 pointings from the high state and 11 pointings in the low state with the source always in the partially coded field-of-view, within 5° from the FOV center. Both Cyg X-1 and SAX J2103.5+4545 (an X-ray pulsar, discovered by Hulleman, in ’t Zand & Heise 1998) are >10° from the FOV center and hence the data are not contaminated by those sources. Source spectra were extracted individually per pointing and then added together into an average ‘high’ and ‘low’ spectrum respectively. The spectra were implicitly background-subtracted by a deconvolution algo-

Table 2. Data from the listed revolutions were used to create the ‘low’ state spectrum. The dates represent the start date of each revolution. The same dates are indicated by filled arrows in Fig. 1. Effective exposure times in ksec are given for each instrument per revolution and in total.

Rev.	start date	JEM-X	ISGRI	SPI
59	2003 – 04 – 08	4	2	–
62	2003 – 04 – 17	–	–	11
67	2003 – 05 – 01	–	–	12
70	2003 – 05 – 10	2	2	11
74	2003 – 05 – 22	4	4	11
79	2003 – 06 – 06	4	4	12
82	2003 – 06 – 15	2	2	11
87	2003 – 06 – 30	2	2	14
142	2003 – 12 – 12	2	2	11
145	2003 – 12 – 21	2	2	11
Total	exposure time :	22	20	104

rithm assuming a spatially flat background. We used the energy range of 3.0–20 keV for spectral fitting. Systematic errors were added as 20% for channels 1–58, 10% for channels 59–96 and 2% for channels 96–255.

2.2. IBIS/ISGRI

For ISGRI, we have selected 54 INTEGRAL pointings for the high state and 10 for the low state with the source always in the totally coded field-of-view. This way we have simultaneous ISGRI and JEM-X data and we do not use the ISGRI partially coded field-of-view for which

the ISGRI response matrix is known to be less accurate. The two different spectral-state set of pointings have been analysed separately. For each set we have produced a mosaicked image (weighted combination of single pointing images) in 10 energy bands. We built the high and soft spectrum extracting the counts/sec from the brightest pixel in each energy band. This method of extracting the spectra from the mosaics instead of adding individual spectra significantly reduces the level of noise and gives high-quality spectra even for low count rates. For the fitting of the two broad-band spectra, we used the energy range 20–150 keV. A 5% systematic error was added to all channels.

2.3. SPI

SPI observations within 15° from the FOV center, from times with similar flux levels at 1.5–12 keV as for the JEM-X and ISGRI data, were selected. The SPI data were analysed using OSA version 3.0, except for some updates due to known problems in the binning software. For image reconstruction and spectral extraction we applied version 6.0 of the SPI Iterative Removal Of Sources program (SPIROS; Skinner & Connell 2003). This allowed us to apply a new background model based on the mean count modulation of the detector array. In order to get precise fluxes, the source positions of the known sources in the field of view have been fixed to their catalogue values. In addition, we allowed SPIROS to apply time dependent normalisation to the source fluxes of the three brightest and variable sources (Cygnus X-1, Cygnus X-3, and EXO 2030+375). Thus the SPI spectrum of Cygnus X-3 presented here is an average over 10 ksec time bins. For spectral extraction, 25 logarithmic bins in the 20–100 keV energy range, and 5 logarithmic bins in 100–2000 keV have been used. The energy range 20–200 keV was used for the spectral fitting due to strong background features at higher energies. The instrumental response function has been derived from on-the-ground calibration (Sturner et al. 2003) and then corrected based on the Crab calibration observation. A 5% systematic error was added to all channels.

The resulting two combined JEM-X, ISGRI and SPI broad-band spectra were fitted using the XSPEC package (Arnaud 1996). The ISGRI and SPI spectra have been renormalized to the JEM-X data. The ISGRI and JEM-X levels showed good agreement while the SPI normalization is a factor of ~ 2 higher. The obtained ‘high’ spectra correspond to the 1.5–12 keV source flux $\gtrsim 200$ mCrab, and the ‘low’ spectra, to $\lesssim 130$ mCrab. Note that neither of these states represent the extreme high/soft or low/hard states displayed by this source on a longer timescale (see §4 below).

3. BROAD-BAND SPECTRAL MODELLING

In spite of a large number of X-ray observations, the spectra of Cyg X-3 have mostly been interpreted in terms of phenomenological models (e.g. Nakamura et al. 1993),

such as power law and bremsstrahlung. The first physical interpretation of the intrinsic broad-band spectrum of Cyg X-3, based on simultaneous *INTEGRAL* (Rev. 23) and *RXTE/PCA-HEXTE* observations in 2002 Dec. 22–23, was given by V03. Their model assumes a hot Comptonizing plasma in the vicinity of an accretion disc, which both provides soft seed photons for the Comptonization and reflects the hard photons emitted by the hot plasma. The specific model, which we also use in this work, is `eqpair` (Coppi 1992, 1999).

In general, the electron distribution in the hot plasma can be purely thermal or hybrid, i.e., Maxwellian at low energies and non-thermal at high energies, if an acceleration process is present. This distribution, including the electron temperature, T , is calculated self-consistently from the assumed form of the acceleration (if present) and from the luminosities corresponding to the plasma heating rate, L_h , and to the seed photons irradiating the cloud, L_s . The plasma optical depth, τ , includes a contribution from e^\pm pairs. The importance of pairs depends on the ratio of the luminosity to the characteristic size, r , which is usually expressed in dimensionless form as the compactness parameter, $\ell \equiv L\sigma_T/(rm_e c^3)$, where σ_T is the Thomson cross section and m_e is the electron mass.

In the fitting process, we have found that our both broad-band *INTEGRAL* spectra are compatible with the hot plasma being completely thermal, and $kT \ll 511$ keV. Then, the e^\pm pair production is negligible, and the absolute value of the compactness is only weakly important. Accordingly, we assume a constant $\ell_s = 10$ (as in V03). We stress, however, that our data, limited to energies $\lesssim 200$ –300 keV, rather weakly constrain possible non-thermal component of the electron distribution and the presence of pairs. Non-thermal processes certainly exist in at least some states of Cyg X-3 (Szostek & Zdziarski 2004; see §4 below).

Our data, covering only photon energies $\gtrsim 3$ keV, rather poorly constrain the form of the seed photons. We therefore use here the same simple assumption as in V03, i.e. emission of an accretion disc with the maximum temperature fixed in the fit. The data also do not allow to constrain the structure of the X-ray absorber and the likely presence of additional spectral components in soft X-rays (e.g. Molnar & Mauche 1986; Nakamura et al. 1993). This absorption and emission is due to the dense wind from the companion Wolf-Rayet star. These processes (which we do not treat in detail here) may strongly affect the spectra up to as much as ~ 20 keV.

For the purpose of modelling the broad-band spectra, we use the same phenomenological model of the absorber as V03. It assumes that one absorbing medium with the column density, $N_{H,0}$, fully covers the source, and another medium with the column, $N_{H,1}$, covers a fraction, f_1 , of the source. We also include Compton reflection (Magdziarz & Zdziarski 1995), parametrized by an effective solid angle subtended by the reflector as seen from the hot plasma, Ω , and assuming an inclination of 60° . We also include an Fe $K\alpha$ fluorescent line, which we model as a Gaussian (with the width of $\sigma_{K\alpha}$, the photon flux of $F_{K\alpha}$, and the peak energy at $E_{K\alpha}$). We allow the reflecting medium (at the assumed temperature

Table 3. Model parameters^a for the two broad-band INTEGRAL spectra of Cyg X-3 in the ‘high’ and ‘low’ state.

Data	$N_{\text{H},0}$ 10^{22} cm^{-2}	$N_{\text{H},1}$ 10^{22} cm^{-2}	f_1	$\ell_{\text{h}}/\ell_{\text{s}}$	τ	kT^{b} keV	$\Omega/2\pi$	ξ^{c} erg cm s^{-1}	$E_{\text{K}\alpha}^{\text{d}}$ keV	$F_{\text{K}\alpha}$ $\text{cm}^{-2} \text{ s}^{-1}$	$F_{\text{bol}}^{\text{e}}$ $\text{erg cm}^{-2} \text{ s}^{-1}$	χ^2/ν
High	20.7 ± 1.4	570 ± 50	0.14 ± 0.11	0.21 ± 0.03	0.21 ± 0.04	73	0.6 ± 0.4	7000^{+3000}_{-7000}	6.61 ± 0.12	0.0085	5.2×10^{-9}	129/172
Low	8.6 ± 7.3	32 ± 21	0.75 ± 0.20	0.22 ± 0.06	0.15 ± 0.13	102	2.0 ± 1.2	3000 ± 1000	6.87 ± 0.07	0.0146	3.8×10^{-9}	129/147

^a The uncertainties are the linear uncertainties as given by XSPEC; the blackbody temperature was fixed at 0.38 keV.

^b Calculated from the energy balance, i.e., not a free fit parameter.

^c Assumed $\leq 10^4$ in the fits.

^d The line photon flux corrected for the Galactic N_{H} only.

^e The bolometric flux of the *absorbed* model spectrum and normalized to the JEM-X/ISGRI data.

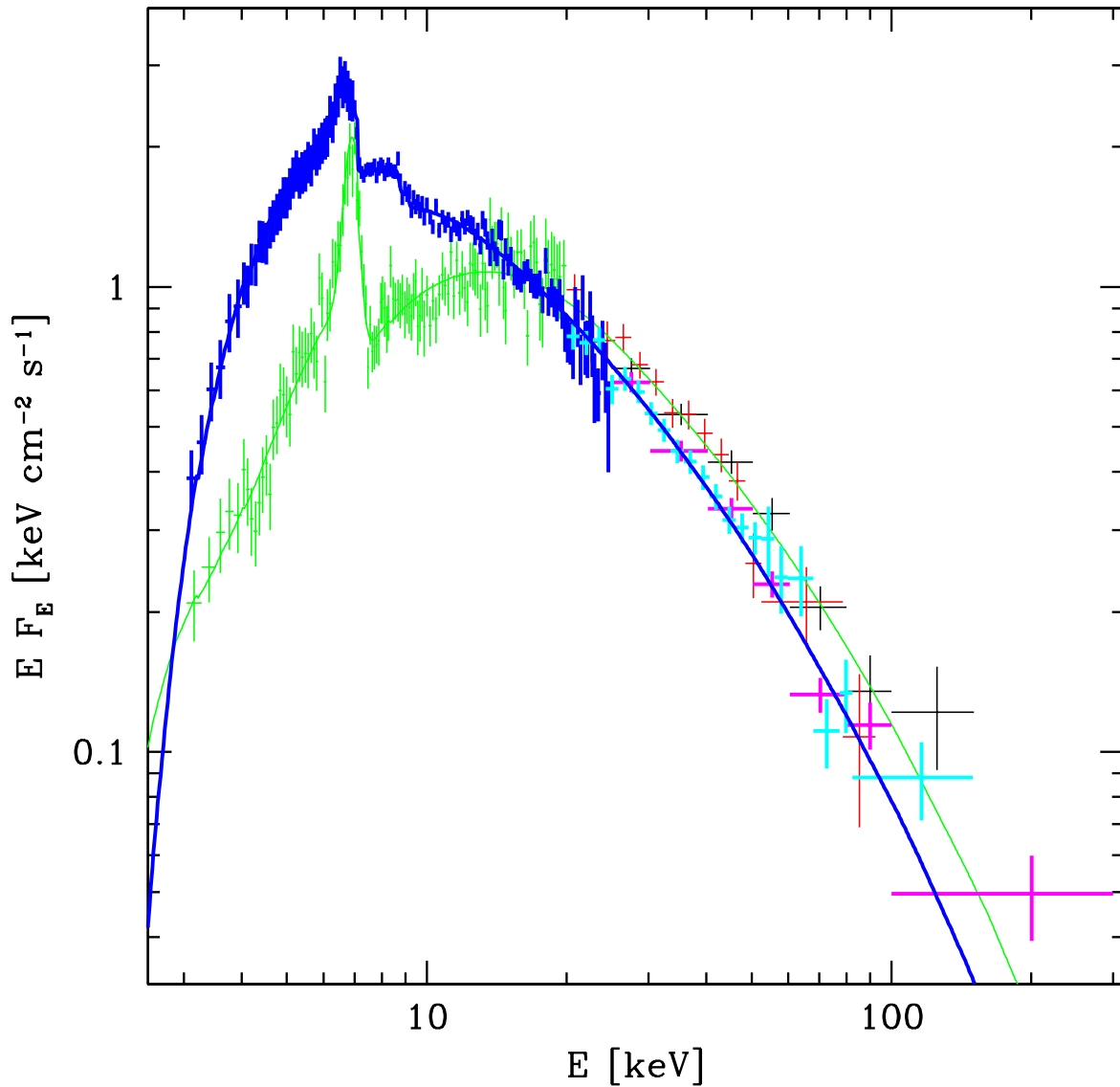


Figure 2. Deconvolved spectra of Cyg X-3. The green, red and black data points correspond to the JEM-X, ISGRI and SPI spectra, respectively, in the high state. The heavy blue, cyan and magenta data points are for the JEM-X, ISGRI and SPI, respectively, in the low state. The model spectra are shown in the green and blue curves. The ISGRI and SPI spectra have been renormalized to the JEM-X data. The proportions of this figure correspond to equal length per decade on each axis.

of 10^6 K) to be ionized, using the ionization calculations of Done et al. (1992). The ionizing parameter is defined as $\xi \equiv 4\pi F_{\text{ion}}/n$, where F_{ion} is the ionizing flux and n is the reflector density. Given the simplified treatment of the ionized reflection of Done et al. (1992), we assume $\xi \leq 10^4$.

The obtained model parameters are given in Table 3, and the deconvolved data and the model spectra are shown in Fig. 2. We see that the two spectra differ strongly at low energies, but their high-energy tails, at energies $\gtrsim 20$ keV, are almost identical, with only a slight difference in the normalization.

4. DISCUSSION

Somewhat surprisingly, the two average spectra obtained by us are very similar at energies above 20 keV, even if there is a clear difference between the shape below 20 keV. We can compare them to the range of the spectra observed so far by the pointed instruments on board *RXTE*. A study of the different spectral states observed by the PCA and HEXTE was performed by Szostek & Zdziarski (2004), who used the same model as that used by us and by V03. Fig. 3 shows four out of five average spectra of Szostek & Zdziarski (2004), with the second hardest spectrum (group #2) omitted for clarity. Those spectra have also been shown by Zdziarski & Gierliński (2004) to be similar to those of the canonical states of black-hole binaries (notwithstanding the peculiar form of absorption in Cyg X-3).

In Fig. 3, we also show the observed ‘low’ and ‘high’ *INTEGRAL* spectra. We find them to be relatively similar in shape to the hard (blue) and intermediate (magenta) average *RXTE* spectra. However, the normalization of the *INTEGRAL* spectra is lower by a factor of ~ 2 . A part of this normalization difference is likely to be due to the different absolute calibration of the JEM-X and ISGRI vs. that of the PCA.

From Fig. 3, we can clearly conclude that with *INTEGRAL*, we have as yet sampled neither the hardest nor the softest spectra of Cyg X-3. Of particular interest here is the ultrasoft state (red spectrum in Fig. 3) with a distinct hard tail. The presence of such a high energy tail without a cutoff below ~ 200 keV requires a nonthermal electron distribution and an acceleration mechanism operating. Due to the fact that the HEXTE detector can measure it only up to ~ 100 keV, the detailed form of this hard tail in the high/ultrasoft state has remained largely unexplored, and it would be of great importance to observe it with *INTEGRAL*. The presence of that tail is clearly accompanied by the very highest level of the flux at 1.5–12 keV, which is also monitored by the *RXTE*/ASM. All ultrasoft spectra corresponding to the average shown in Fig. 3 were observed when the ASM flux level was > 27 counts/sec, which corresponds to > 360 mCrab. In comparison, see the right panel of Fig. 1, the highest flux levels observed during the lifetime of *INTEGRAL* have only occasionally reached above 20 counts/sec and *INTEGRAL* has thus yet not been able to observe a true high/ultrasoft state of Cyg X-3.

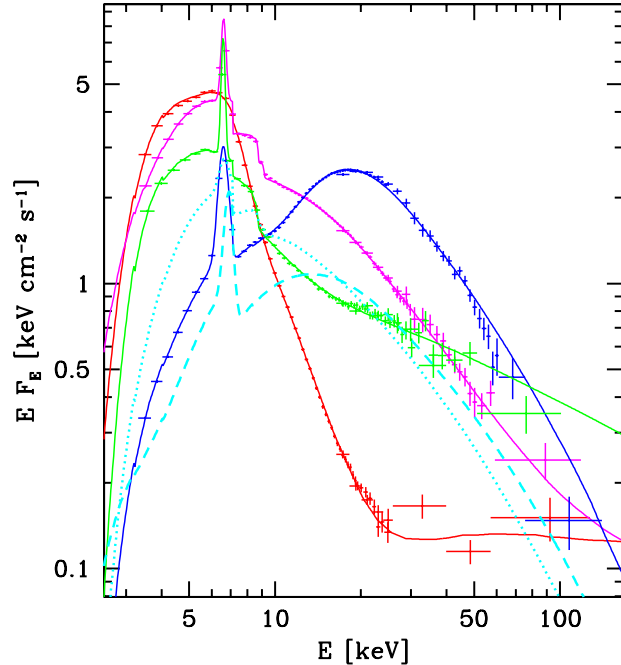


Figure 3. The range of spectra observed so far by *RXTE*/PCA/HEXTE compared to the present *INTEGRAL* spectra. The red, magenta, green and blue spectra represent four out of five groups obtained by Szostek & Zdziarski (2004) by averaging 42 *RXTE* observations from 1996–2000 (normalized to the PCA). The low and high *INTEGRAL* spectral models are plotted in the dashed and dotted cyan curves, respectively.

5. CONCLUSIONS

We have combined multiple JEM-X, ISGRI and SPI spectra from available public and GPS observations to create two broad-band spectra of Cyg X-3, corresponding to high and low levels of the 1.5–12 keV flux. The resulting ‘high’ and ‘low’ spectra resemble what can be referred to as the intermediate and the low/hard state of this source, but are similar in shape above 20 keV. We have fitted the intrinsic spectra with thermal Comptonization models including Compton reflection, which are (see Zdziarski & Gierliński 2004) similar to those found for black-hole binaries. We point out that *INTEGRAL* has yet to observe Cyg X-3 in the high/ultrasoft state, which would provide a very interesting opportunity to study the hard non-thermal tail associated with this state.

ACKNOWLEDGMENTS

This research has been based on observations with *INTEGRAL*, an ESA project with instruments and science data center funded by ESA and member states (especially the PI countries: Denmark, France, Germany, Italy, Switzerland, and Spain), the Czech Republic, and Poland and with the participation of Russia and the US. It has also made use of data obtained through the HEASARC Online Service (provided by NASA/GSFC), and of NASA’s

Astrophysics Data System. The authors from the Observatory of the University of Helsinki acknowledge the Academy of Finland, TEKES, and the Finnish space research programme ANTARES for financial support. AAZ has been supported by KBN grants 5P03D00821, 2P03C00619p1,2 and PBZ-KBN-054/P03/2001.

REFERENCES

Arnaud, K. A. 1996, in ASP Conf. Ser. Vol. 101, Astronomical Data Analysis Software and Systems V, eds. Jacoby G. H., Barnes J. (San Francisco: ASP), 17

Choudhury,M., Rao,A.R., Vadawale,S.V. et al. 2002, A&A, 383, L35

Coppi, P. S. 1992, MNRAS, 258, 657

Coppi, P. S. 1999, in ASP Conf. Ser. Vol. 161, High Energy Processes in Accreting Black Holes, eds. J. Poutanen & R. Svensson (San Francisco: ASP), 375

Courvoisier, T. J.-L., Walter, R., Beckmann, V., et al. 2003, A&A, 411, L53

Done, C., Mulchaey, J. S., Mushotzky, R. F., & Arnaud, K. A. 1992, ApJ, 395, 275

Ergma, E. & Yungelson, L. R., 1998, A&A, 333, 151

Giacconi, R., Gorenstein, P., Gursky, H. & Waters, J. R. 1967, ApJ, 148, L119

Hulleman, F., in 't Zand, J. J. M., & Heise, J. 1998, A&A, 337, L25

Magdziarz, P., & Zdziarski, A. A. 1995, MNRAS, 273, 837

McCollough, M. L., Robinson, C. R., Zhang, S. N., et al. 1999, ApJ, 517, 951

Molnar, L. A., & Mauche, C. W. 1986, ApJ, 310, 343

Nakamura, H., Matsuoka, M., Kawai, N., et al. 1993, MNRAS, 261, 353

Predehl,P., Burwitz,V., Paerels,F., Trumper,J., 2000, A&A, 357, L25

Schmutz, W., Geballe, T. R., & Schild, H. 1996, A&A, 311, L25

Singh, N. S., Naik, S., Paul, B., et al. 2002, A&A, 392, 161

Skinner, G., & Connell, P. 2003, A&A, 411, L123

Stark, J., & Saia, M. 2003, ApJ, 587, L101

Sturner, S. J., Shrader, C. R., Weidenspointner, G., et al. 2003, A&A, 411, L81

Szostek, A. & Zdziarski, A. A., 2004, in X-ray Timing 2003: Rossi and Beyond, eds. P. Kaaret, F. K. Lamb and J. H. Swank (American Institute of Physics, Melville, NY) in press

van Keerkwijk, M. H., et al. 1992, Nature, 355, 703

van Keerkwijk, M. H., et al. 1996, A&A, 314, 521

Vilhu, O., Hjalmarsson L., Zdziarski A. A., et al. 2003, A&A, 411, L405

Watanabe,H., Kitamoto,S., Miyamoto,S. et al. 1994, ApJ, 433, 350

White, N. E., & Holt, S. S. 1982, ApJ, 257, 318

Zdziarski, A. A., & Gierliński, M., 2004, Prog. Theor. Phys., in press